IOP Publishing Journal of Physics: Condensed Matter
J. Phys.: Condens. Matter **32** (2020) 275701 (11pp) https://doi.org/10.1088/1361-648X/ab7d65

# Disorder-robust bands from anisotropic orbitals in a coordination polymer semiconductor

**Daniel M Packwood**[1] **and Pichaya Pattanasattayavong**[2,3]

[1] Institute for Integrated Cell-Material Sciences (iCeMS), Kyoto University, Kyoto, Japan
[2] Department of Materials Science and Engineering, School of Molecular Science and Engineering, Vidyasirimedhi Institute of Science and Technology (VISTEC), Rayong, Thailand
[3] Research Network of NANOTEC-VISTEC on Nanotechology for Energy, Vidyasirimedhi Institute of Science and Technology (VISTEC), Rayong, Thailand

E-mail: dpackwood@icems.kyoto-u.ac.jp

Received 2 December 2019, revised 25 February 2020
Accepted for publication 6 March 2020
Published 7 April 2020

**Abstract**

While the effects of structural disorder on the electronic properties of solids are poorly understood, it is widely accepted that spatially isotropic orbitals lead to robustness against disorder. In this paper, we use first-principles calculations to show that a cluster of occupied bands in the coordination polymer semiconductor $\beta$-copper(I) thiocyanate undergo relatively little fluctuation in the presence of thermal disorder—a surprising finding given that these bands are composed of spatially anisotropic d-orbitals. Analysis with the tight-binding method and a stochastic network model suggests that the robustness of these bands to the thermal disorder can be traced to the way in which these orbitals are aligned with respect to each other. This special alignment causes strong inverse statistical correlations between orbital–orbital distances, making these bands robust to random fluctuations of these distances. As well as proving that disorder-robust electronic properties can be achieved even with anisotropic orbitals, our results provide a concrete example of when simple 'averaging' methods can be used to treat thermal disorder in electronic structure calculations.

Keywords: coordination polymer semiconductor, band structure, thermal disorder, density functional theory, tight-binding model, stochastic model

Supplementary material for this article is available online

(Some figures may appear in colour only in the online journal)

## 1. Introduction

With the availability of fast electronic structure codes and abundant computational resources, reliable electronic band structures of solid-state materials can now be computed routinely. However, while a wealth of insights related to charge transport have been obtained from such calculations, the overwhelming majority of reported band structures assume that thermal disorder, arising from the thermal motions of the atoms, is entirely absent in the system [1, 2]. While this assumption is tolerable for materials held together by rigid covalent bonds, it is questionable for materials held together by weaker interactions, such as metal–ligand coordination bonds. Unfortunately, the effects of thermal disorder on band structure in such materials remain unclear at present.

One of the simplest methods for incorporating thermal disorder into band structure calculations is to simulate the equilibrium dynamics of the material at the temperature of interest (using molecular dynamics simulation or Monte Carlo sampling), and average the band structure over the frames of simulation [3–5]. While this method cannot predict qualitative changes of the charge transport mechanism, such as a transition from band transport to thermally activated hopping transport, it is useful for exploring charge carrier

 

localization, direct-to-indirect transitions, and band gap narrowing are induced by thermal disorder. On the other hand, because thermal disorder is dynamic, this 'averaging' method is only meaningful when the time-dependent fluctuations of the band energies about their average value are very small.

For the special cases in which band energies and other electronic properties are insensitive to disorder (due to thermal motions, static disorder, or otherwise), it is widely believed that the insensitivity arises from spatially isotropic *s* orbitals [6–9]. This idea, which arises particularly in the context of non-crystalline semiconductors (such as $2CdO{\cdot}GeO_2$ and IGZO [10, 11]), follows from the fact that overlap integrals between pairs of isotropic orbitals only depend upon the distances between orbitals, and not upon their relative orientation. Providing that large variations in the inter-orbital distances do not occur, electronic bands and conduction pathways composed of isotropic orbitals should not be strongly affected by the disorder. In the presence of thermal disorder, the energies of such bands should, therefore, show little fluctuation about their average values. While this idea is insightful and certainly reasonable, the requirement of isotropic orbitals restricts it to a narrow class of materials. For the purpose of understanding when the averaging method described in the previous paragraph can be meaningfully applied, it is useful to consider whether small fluctuations could be possible for bands composed of anisotropic orbitals as well.

In order to understand how band energies or other electronic properties fluctuate in the presence of thermal disorder, it is helpful to consider two contributions: the OO (orbital orientation) contribution, which arises from orientation fluctuations of the orbitals, and the OD (orbital distance) contribution, which arises from distance fluctuations between orbitals. For the case of bands arising from isotropic orbitals, the OO contribution is minimized and large band energy fluctuations can only arise from fluctuations in the orbital–orbital distances. In this paper, we show that the opposite situation—where the OD contribution is minimized, and large band energy fluctuations can only arise from fluctuations in orbital orientations—can also be realized. More specifically, we use first-principles calculations to predict a cluster of occupied bands in the coordination polymer semiconductor $\beta$-copper(I) thiocyanate (CuSCN) [12–16] whose energies show remarkably little fluctuation in the presence of thermal disorder. These bands are referred to as 'hole-transporting bands', due to the fact that they reside close to the valance band edge and that CuSCN is a p-type semiconductor. The negligible fluctuations of the hole-transporting bands is unintuitive because they are composed of anisotropic Cu d orbitals which are not expected to lead to a negligible OO contribution as described above. By constructing a simple tight-binding model for the hole-transporting bands, we find that the d-orbitals in CuSCN are aligned in such a way that highly directional $\sigma$-type interactions between neighbors dominate in the hole-transporting bands. Analysis of a stochastic network model then shows a surprising result: that this specific type of d-orbital alignment causes the OD contribution to the band fluctuations to become very small. As well as proving that disorder-insensitive electronic properties can be achieved even with anisotropic orbitals, this result provides a specific condition under which the simple 'averaging' method described above can be meaningfully applied to understand how thermal disorder affects band structure.

## 2. Fluctuations of the hole-transporting bands due to thermal disorder

A mixture of plane-wave density functional theory (DFT) and Markov chain Monte Carlo (MCMC) calculations were performed in order to study the effects of thermal disorder the CuSCN band structure. All calculations in this section used a $2 \times 2 \times 1$ supercell of CuSCN. Plane-wave DFT calculations were performed using the Vienna *Ab Initio* Simulation Package (VASP) [17] with the PBE exchange–correlation functional [18]. Single-point energy calculations (performed during the MCMC simulations) used a 450 eV basis set cut-off and $\Gamma$-centered $2 \times 2 \times 1$ $k$-points grids. Density of states calculations were performed with $12 \times 12 \times 8$ $k$-points grids and 640 eV basis set cut-offs. Band structure calculations were performed with 640 eV basis set cut-offs and 100 $k$-points divisions between high-symmetry points. The $2 \times 2 \times 1$ supercell was relaxed from a single unit cell starting from the experimental structure [16]. MCMC simulations were performed using an in-house R code [19] interfaced with VASP. Trial moves were obtained by adding Gaussian noise to all atomic coordinates, and the ordinary Metropolis criterion was used to accept or reject atomic configurations. MCMC simulations were performed for $2 \times 10^5$ steps. Under these settings and with our computational resources, around two months were required to complete the MCMC simulations and perform all band structure calculations. When analyzing the output of the MCMC simulations, the first $5 \times 10^4$ steps were removed to minimize artifacts arising from the equilibration phase, and $10^4$ snapshots of the system were randomly selected from the remaining steps for subsequent analysis. Principal components were computed using the prcomp command from R [19].

The major principal components of the atomic motion at 298 K, as predicted by our calculations, are displayed in figure 1. Principal components represent collective modes of motion in the crystal [20], and the ones which are shown in figures 1(A)–(C) are the three modes which account for the majority of the thermal motion observed in our calculations. It can be seen that all atoms in the crystal, including copper, undergo large and incoherent motions at 298 K. In fact, copper atoms have mean square displacement of 0.035 $Å^2$, compared 0.027 $Å^2$ for all atoms (averaged over all directions), showing that Cu tends to undergo slightly larger displacements than the other atoms. The large motions of the Cu atoms can be further confirmed by the boxplots in supporting information I (stacks.iop.org/JPhysCM/32/275701/mmedia).

The 0 K band structure for the CuSCN supercell is shown in supporting information II. In agreement with the band structures calculated by other authors [21, 22], it has a valance band maximum at the $\Gamma$ point, conduction band minimum at the $K$ point, and an indirect band gap of 2.12 eV. Another conduction band minimum at the $\Gamma$ point also exists, which is only 0.06 eV higher in energy than the minimum at the $K$-point.

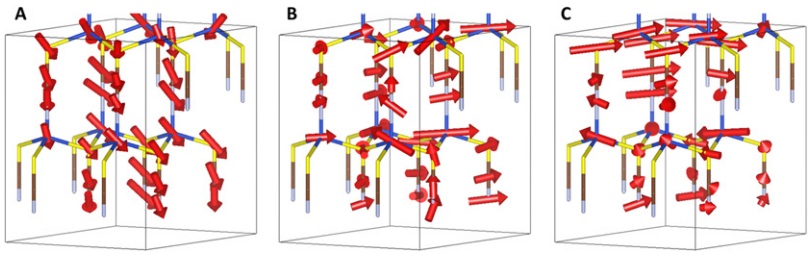


**Figure 1.** $2 \times 2 \times 1$ supercell of $\beta$-copper thiocyanate (CuSCN) (stick representation). Blue, light blue, brown, and yellow represent copper, nitrogen, carbon, and sulfur atoms, respectively. The red arrows show the 'principal components' of the thermal atomic motion at 298 K. Principle components can be interpreted as collective modes of atomic motion at thermal equilibrium. There are 96 principal components possible for this system, and figures (A–C) show the ones which account for the most, second most, and third most of the variation in the atomic positions at equilibrium, respectively.

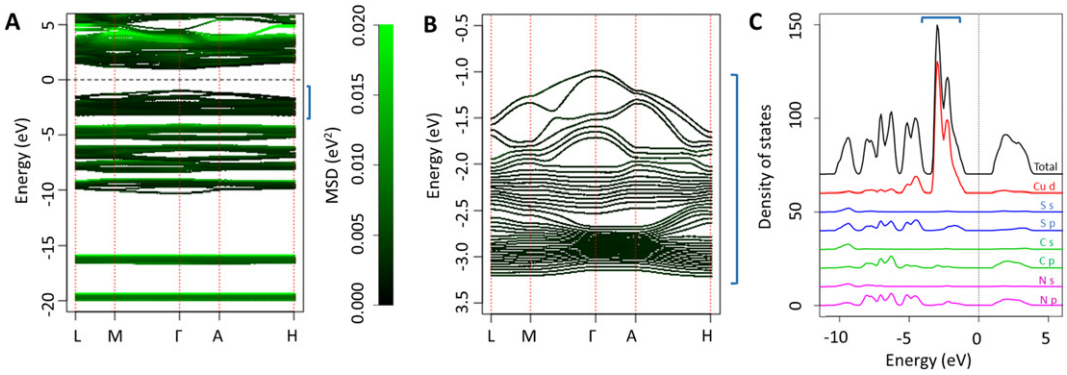


**Figure 2.** (A) Thermally averaged band structure for a $2 \times 2 \times 1$ supercell of CuSCN at 298 K. The green color corresponds to the mean-square displacement (MSD) of the band energies from their average values. The 'hole bands' are indicated by the blue bracket on the right-hand side. The Fermi level is marked by the dotted line. (B) As for A, but zoomed-in on the hole bands. (C) Thermally averaged total (black) and orbital-projected (colored) density of states for a $2 \times 2 \times 1$ supercell of CuSCN at 298 K. The 'hole bands' are indicated by the blue bracket at the top. The Fermi level is marked by the dotted line.

The band gap of 2.12 eV is smaller than the experimental band gap of 3.7–3.9 eV [12], however this problem is expected because the DFT calculation was performed with the generalized gradient approximation [23]. Calculations using the hybrid functional HSE06 reported by other authors have predicted band gaps between 3.00 eV and 3.45 eV, but without notable changes to the band structure compared to that obtained using the generalized gradient approximation [22, 24]. Figure 2(A) plots the time-averaged folded band structure of the CuSCN supercell at 298 K (supporting information III shows the same plot over a longer Brillouin zone path). This band structure has been obtained by averaging over 100 snapshots from the MCMC simulations. Despite the superficial appearance of more bands (due to thermal disorder breaking band degeneracy), the averaged band structure is qualitatively comparable to the 0 K band structure, showing a valance band maximum at the Γ point. However, the conduction band minimum at the Γ point sinks below the one at the *K* point, leading to a direct band gap of 1.97 eV. This band gap grows to 2.05 eV at the reduced temperature of 150 K, which further verifies the temperature dependence of the band structure. This inverse relationship between band gap and temperature is consistent with the general properties of semiconductors [25].

In figure 2(A), the bands are colored according to the extent to which they fluctuate about their average value at 298 K, with black and green representing weakly fluctuating and strongly fluctuating parts of the band structure, respectively. The extent of the fluctuations is quantified by their mean-square displacement from their average value. In contrast to many other bands, it can be seen that the series of bands just below the Fermi level (the 'hole bands') undergo conspicuously little fluctuation. The hole bands are plotted in more detail in figure 2(B). Figure 2(C) plots the orbital-projected density of states of these bands, showing that they are formed almost entirely from the Cu d orbitals, with some minor contributions from the S p orbitals. The dominance of Cu 3d states has also been substantiated experimentally by photoelectron spectroscopy [13]. The lack of large fluctuations of the hole bands in the presence of thermal disorder is surprising, given the anisotropic shapes of the d orbitals involved. This result becomes more surprising when we recall figure 1, which showed that the Cu atoms exhibit large thermal motions.

## 3. Tight-binding model for the hole bands

In order to explain the absence of large energy fluctuations in the CuSCN hole bands in the presence of thermal disorder, we need to examine the atomic orbital interactions in these bands in more detail. Unfortunately, plane-wave DFT calculations are not so useful for this purpose, because the plane-wave basis set does not allow us to quantify interactions between atomic orbitals. We, therefore, construct a tight-binding model

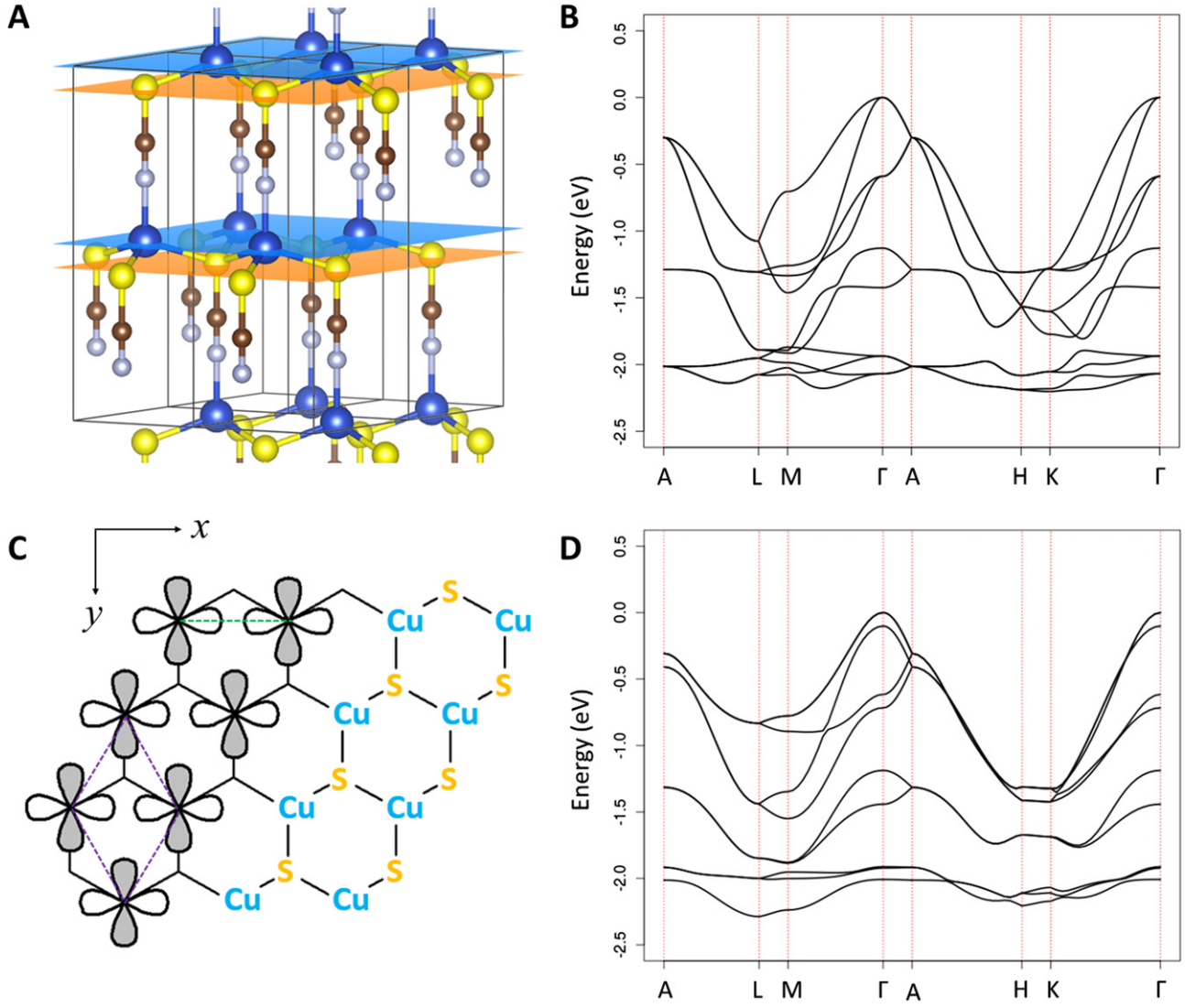


**Figure 3.** (A) Ball-and-stick structure of CuSCN with unit cells indicated by the black lines. Cu and S atomic planes are indicated by the blue and orange planes, respectively. (B) Hole bands for CuSCN (single unit cell) computed from density functional theory. (C) Tight-binding model composed of Cu d-orbitals which are coupled predominantly via in-plane $\sigma$-interactions, and (D) the corresponding band structure. The dotted green and purple lines indicate two-way ('A-type') and four-way ('B-type') $\sigma$-interactions, respectively. As a guide for the eye, the Cu and S atoms have been colored to match the atomic plane colors in (A).

for the CuSCN hole bands. While the tight-binding model is too simple to give an accurate description of the hole bands, its parameters directly quantify the strength of the atomic orbital interactions, allowing us to clearly visualize the bonding in the CuSCN hole bands and analyze how they respond to the thermal disorder.

In order to ensure a minimal model for the hole bands, we only consider Cu d orbitals when constructing the tight-binding model. To construct the model, we note that the structure of CuSCN consists of layers of Cu atoms, and that the unit cell contains two Cu atoms from adjacent layers. (figure 3(A)). Referring to these layers as $L_1$ and $L_2$, respectively, we write the state of a single unit cell as a linear combination of Cu d orbitals, namely

$$|\mathbf{r}_j\rangle = \sum_{\mu=1}^{5} \left( c_\mu^{L_1} |\mu, \mathbf{r}_j, L_1\rangle + c_\mu^{L_2} |\mu, \mathbf{r}_j, L_2\rangle \right), \qquad (1)$$

where $\mathbf{r}_j$ is the position vector for the unit cell, $|\mu, \mathbf{r}_j, L_1\rangle$ and $|\mu, \mathbf{r}_j, L_2\rangle$ represent d-orbitals with magnetic quantum number $\mu$ localized on the Cu atom from layers $L_1$ and $L_2$, respectively. The state of the system is given by the Bloch sum $|\mathbf{k}\rangle = \Sigma_j \exp(i\mathbf{k}\cdot\mathbf{r}_j)|\mathbf{r}_j\rangle$. Our Hamiltonian $H$ contains terms for intra-layer and inter-layer coupling between d orbitals, and only nearest-neighbor couplings are considered (see appendix A and figure A1 for details). In order to determine the Hamiltonian matrix elements for our model, we apply the Slater–Koster method [26] (see [27] for a recent application of this method). This introduces 11 free parameters into the model, which can be interpreted as orbital energies and orbital interaction strengths. These parameters were fit by minimizing the square deviation of the tight-binding model band energies from those of the 0 K band structure calculated by DFT (figure 3(B)) at the high symmetry points of the Brillouin zone. The fitted parameter values are shown in

**Table 1.** Parameters for the tight-binding model. The parameters $(dd\sigma)$, $(dd\pi)$, and $(dd\delta)$ refer to $\sigma$-, $\pi$-, and $\delta$-interaction strengths, respectively. Subscripts 0 and 1 denote the in-plane and between-plane interactions, respectively. All quantities are in eV. After computing the band structure these parameters, it was shifted so that the valance band maximum was at 0 eV.

| $(dd\sigma)_0$ | $(dd\pi)_0$ | $(dd\delta)_0$ | $(dd\sigma)_1$ | $(dd\pi)_1$ | $(dd\delta)_1$ |
|---|---|---|---|---|---|
| 0.228 | 0.060 | −0.021 | −0.035 | −0.001 | 0.06 |

supporting information VI and V, with the values for the orbital interactions shown in table 1. The corresponding band structure plotted in figure 3(D). The agreement between the tight-binding model band structure and the DFT-calculated band structure is good considering the simplicity of the model. The tight-binding model band structure captures all qualitative features of the hole bands (valance band maximum at the Γ point and a series of weakly dispersive bands at lower energies), although it overestimates the band energies at the corners of the Brillouin zone.

By interpreting the parameters of the tight-binding model, we can ascertain how the orbitals are coupled in the hole bands. According to table 1, the Cu atoms within the layers are coupled predominantly via $\sigma$-interactions, whereas the Cu atoms between layers are coupled via a mixture of $\sigma$- and $\delta$-interactions. This situation can be realized by considering one $d_{x2-y2}$ orbital on each Cu atom aligned as shown in figure 3(C). With the $d_{x2-y2}$ orbitals aligned in this way, we can see that two types of $\sigma$-interactions within the layers are possible: 'A-type' interactions (shown by the dotted green line) and 'B-type' interactions (shown by the dotted purple lines). The A-type interactions will dominate over the B-type interactions, due to the favorable alignment of the orbitals for $\sigma$-interaction. The contribution of the $d_{xy}$, $d_{yz}$ and $d_{xz}$ orbitals can be ignored, because these lead to in-plane $\pi$- and $\delta$-interactions, which are of relatively little importance according to table 1. The $\sigma$- and $\delta$-interactions between layers can be accounted for by the $d_{z2}$ and $d_{x2-y2}$ orbitals, respectively.

## 4. Analysis with a stochastic network model

In order to explain how the orbital arrangement shown in figure 3(C) might lead to band robustness to thermal disorder, we analyzed band fluctuations on the basis of a stochastic network model. This model describes how fluctuations in the distances between neighboring d-orbitals contribute to the fluctuations of the band energies. If we suppose that the mean-square energy displacement of the hole bands at $k$-point $\mathbf{k}$ can be written as

$$\mathrm{MSE}\,(\mathbf{k}) = \mathrm{OD}\,(\mathbf{k}) + \mathrm{OO}\,(\mathbf{k}), \tag{2}$$

where OD measures the contribution arising from distance fluctuations between orbitals, and OO measures the contribution arising from orbital orientation fluctuations, then the stochastic network model can be used to understand OD.

The stochastic network model, which is a quantum version of the one presented in reference [28], consists of a finite number of nodes and connections between nodes (figure 4(A)). The nodes correspond to Cu atoms, and a connection between nodes represents an interaction between the orbitals of the two atoms. The nodes are positioned in exactly the same way as the copper atoms from a single copper plane of CuSCN. At present, we do not include additional planes in the model, because the interaction between planes is not expected to be significant compared to in-plane interactions. Only nearest-neighbor connections are included in the network. We assume that only one orbital resides at each node, and let $|\alpha\rangle$ denote the orbital residing at node $\alpha$. The ground state of the system is assumed to be

$$|\psi\rangle = \sum_{\alpha} c_\alpha |\alpha\rangle, \tag{3}$$

where the index $\alpha$ runs over all nodes, $|\alpha\rangle$ denotes an orbital located at node $\alpha$, and all coefficients $c_\alpha$ are real-valued and have the same sign. The latter implies that $|\psi\rangle$ is a bonding orbital. The energy of the system, $E$, can be found by computing $E = \langle\psi|H|\psi\rangle$, where the Hamiltonian $H$ is

$$H = \sum_{\alpha} \varepsilon_\alpha \,|\alpha\rangle\,\langle\alpha| + \sum_{\alpha\sim\beta} g_{\alpha\beta}\,|\alpha\rangle\,\langle\beta|\,, \tag{4}$$

where $\varepsilon_\alpha$ is the energy of the orbital at node $\alpha$, $g_{\alpha\beta}$ measures the coupling strength between orbitals from connected pairs of nodes $\alpha$ and $\beta$, and the second sum runs over all pairs of connected nodes. We further assume that the orbital energies are constant (i.e., $\varepsilon_\alpha = \varepsilon$). On the other hand, the coupling strengths are assumed to explicitly depend upon the distances $r_{\alpha\beta}$ between nodes, i.e.,

$$g_{\alpha\beta} = g\left(r_{\alpha\beta}\right). \tag{5}$$

$g_{\alpha\beta}$ is identical for all connections, because $r_{\alpha\beta}$ is fixed at 3.85 Å for all connections in the network in figure 4(A). In passing, note that the Hamiltonian in (3) differs from the one used in the tight-binding model in the previous section, due to the different assumptions involved.

We wish to understand how the energy of the system is affected by random atomic disorder. To incorporate atomic disorder into the model, we add a Gaussian random vector to each node. This causes the position of node $i$ to change from $\mathbf{r}_i$ to $\mathbf{r}_i + \mathbf{X}_i$, where the Gaussian random vector $\mathbf{X}_i$ has components with the average value of zero and standard deviation $\sigma$. As a result of this disorder, the coupling strengths become

$$g'_{\alpha\beta} = g_0 + R_{\alpha\beta}\Delta r_{\alpha\beta} \tag{6}$$

where $g_0 = g(r_{\alpha\beta} = 3.85\ \text{Å})$ is the initial coupling strength, $\Delta r_{\alpha\beta}$ is the change in the $\alpha$–$\beta$ distance due to the random disorder, and $R_{\alpha\beta}$ measures the sensitivity of the coupling strength to changes in distance (concretely, $R_{\alpha\beta} = \mathrm{d}g(r_{\alpha\beta} + \Delta r_{\alpha\beta})/\mathrm{d}\Delta r_{\alpha\beta}|_{\Delta r\alpha\beta\,=\,0}$). Assuming that the disorder is not too large (or equivalently, that $\sigma^2$ is small), the $\Delta r_{\alpha\beta}$ can be treated as first-order perturbations. Accordingly, we find that the energy of the system in the presence of disorder is $E + E'$. We find that, $E'$ has an average value of zero and mean-square

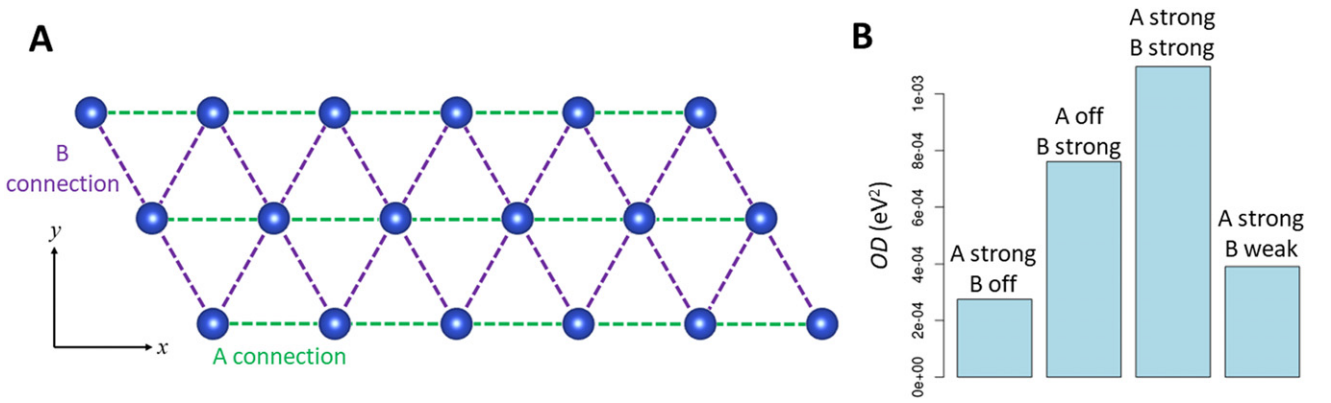


**Figure 4.** (A) Illustration of the stochastic network model. Blue spheres correspond to nodes, which are positioned in the same way as the Cu atoms from a single Cu plane of CuSCN. A single orbital is located at each node, and the connections (dotted lines) indicate orbital–orbital interactions between nodes. A-type (green) and B-type (purple) connections are shown. (B) Contribution of inter-orbital distance fluctuations to the band energy fluctuation, as computed with the stochastic network model. 'A strong B off' means that the calculation was performed with B connections deleted from the network. 'A off B strong' means that A connections were deleted from the network. 'A strong, B strong' means that both connections were present in the network. 'A strong B weak' means that both connections were present in the network, but that the orbital–orbital interactions represented by B connections were weakened. Calculation parameters (see text): $\sigma = 1$ Å, initial coupling strength $= -1$ eV (strong connections), $-0.25$ eV (weak connections), coupling strength sensitivities $=$ 0.1 eV Å$^{-1}$ (strong connections), 0.025 eV Å$^{-1}$ (weak connections).

displacement from zero given by (see appendix B)

$$\mathrm{OD} = 2\sigma^2 \sum_{\alpha\sim\beta} c_\alpha^2 c_\beta^2 R_{\alpha\beta}^2 + \sigma^2 \sum_{\alpha\sim\beta\sim\gamma} c_\alpha c_\beta^2 c_\gamma R_{\alpha\beta} R_{\beta\gamma} \cos\,\chi_{\alpha\beta\gamma} \tag{7}$$

In equation (7), the first sum runs over all pairs of connected nodes, and the second sum runs over all triplets of nodes $\alpha$, $\beta$, and $\gamma$ connected sequentially (where $\alpha$ is connected to $\beta$ and $\beta$ connected to $\gamma$). $\chi_{\alpha\beta\gamma}$ is the angle $\alpha\beta\gamma$. Note that OD in equation (7) does not depend upon the wave vector $\mathbf{k}$ because the stochastic network model is not periodic and only considers a finite number of nodes. Nonetheless, the behavior of OD in equation (7) should be analogous to the behavior of OD($\mathbf{k}$) in equation (2).

To compute OD, we divide these connections into one of two types (figure 4(A)). 'A-type' connections, which run parallel to the $x$-axis, and 'B-type' connections, which project between the $x$ and $y$ axes. We then compute the OD term for the following four regimes: (i) 'A strong B off', which means that the calculation was performed with B-type connections deleted from the network, (ii) 'A off B strong' which means that A-type connections were deleted from the network, (iii) 'A strong B strong', which means that both types of connections were present in the network, and (iv) 'A strong B weak', which means that both connections were present in the network, but the strength of the B-type connections was weakened. The parameter choices corresponding to these regimes are given in the caption of figure 4. The technical details are discussed in appendix C. As figure 4(B) shows, OD smallest in the 'A strong B off' regime, and second smallest in the 'A strong B weak regime'. Thus, the OD term tends to minimize as A-type connections dominate over B-type connections.

The result in figure 4(B) helps explain the robustness of the hole bands in CuSCN. As discussed in the previous section, the tight-binding model predicted that the within-layer d-orbital interactions were predominantly of the A-type, with a smaller contribution from the B-type (figure 3(B)). Subsequently, the stochastic network model shows that the OD contribution to band energy fluctuations is minimized for the case of only A-type connections, and becomes only somewhat larger when weak B-type connections are included. This result therefore suggests that the stability of the hole bands might be traced to the special way in which the d-orbitals in CuSCN are aligned, in which A-type connections dominate. This special alignment means that fluctuations in the relative orbital distances do not cause large band energy fluctuations. Instead, large band fluctuations can only occur due to fluctuations in the relative orbital orientations (as described by the OO term).

To understand how A-type connections might suppress band energy fluctuations, we examine equation (7) in detail. In equation (7), the first term arises from fluctuations of the distances between pairs of nodes, and is always positive in value. The second term arises from statistical correlations between these fluctuations, and can have a positive or negative value. Importantly, this correlation will not be zero. For example, consider three nodes $\alpha$, $\beta$, and $\gamma$ connected sequentially, and let $r_{\alpha\beta}$ and $r_{\beta\gamma}$ denote the distances between nodes $\alpha$ and $\beta$ and $\beta$ and $\gamma$, respectively. Then, if the node $\beta$ is shifted due to atomic disorder, both $r_{\alpha\beta}$ and $r_{\beta\gamma}$ will change simultaneously and non-independently. This implies a statistical correlation between $r_{\alpha\beta}$ and $r_{\beta\gamma}$. Moreover, it can be shown that this statistical correlation is proportional to cos $\chi_{\alpha\beta\gamma}$ (see appendix B, equation (B.17)). Now, for the case of predominantly A-type interactions between d-orbitals, as in the hole bands of CuSCN, B-type interactions can be ignored, and we have the extreme situation where $\chi_{\alpha\beta\gamma} = \pi$ for all angles and all cos $\chi_{\alpha\beta\gamma} = -1$. This causes the second term in equation (7) to become strongly negative, and makes the OD term small. Thus, the small OD contribution to the band energy fluctuations in

CuSCN must arise from strong negative statistical correlations between the orbital–orbital distances during the random atomic fluctuations.

The physical picture behind these negative statistical correlations is as follows. As before, consider three nodes $\alpha$, $\beta$, and $\gamma$ connected sequentially, let $r_{\alpha\beta}$ and $r_{\beta\gamma}$ denote the distances between nodes. In the case of only A-type connections, in which $\chi_{\alpha\beta\gamma} = \pi$ for all connected nodes, it is unlikely that random fluctuation would cause both $r_{\alpha\beta}$ and $r_{\beta\gamma}$ to increase simultaneously. In order for this to happen, $\beta$ would need to be displaced in a direction nearly perpendicular to the connections, which unlikely when the displacement is random. Moreover, it is not possible for a random fluctuation to cause both $r_{\alpha\beta}$ and $r_{\beta\gamma}$ to decrease simultaneously. The probability that $r_{\alpha\beta}$ and $r_{\beta\gamma}$ can be both large or both small at the same time is therefore reduced, which implies a negative correlation between $r_{\alpha\beta}$ and $r_{\beta\gamma}$.

While this analysis strongly suggests that the lack of large fluctuations in the hole bands of CuSCN is due to the minimized OD contribution, we do not attempt to compare the size of OD and OO contributions in the present work. Nonetheless, this shortcoming does not affect our conclusions that the hole band energies in CuSCN are robust to distance fluctuations between orbitals, and that large energy fluctuations can only be due to orbital orientation fluctuations. In future research, we will attempt to create a simple model to understand the OO contribution in detail. This should allow us to compare the OO and OD terms directly and determine whether the hole band energies are robust to fluctuations in orbital orientation as well.

## 5. Conclusions

Band structure averaging, one of the simplest methods for incorporating the effects of thermal disorder into band structure calculations, is most applicable when the fluctuations of the band energies about their average value are small. While such fluctuations are expected to be minimized for the case of bands formed from spatially isotropic orbitals, it is desirable to elucidate other situations in which the fluctuations are small as well. In the work above, we used first-principles calculations to predict that a cluster of hole-transporting bands in the coordination polymer semiconductor CuSCN exhibit remarkably little fluctuation in the presence of thermal disorder, despite being composed of anisotropic d orbitals. Analysis of the band structure with two simple models (tight-binding model and the stochastic network model) suggested that the lack of fluctuations is due to the special row-like alignment of the d-orbitals in these bands. This special row-like alignment causes the orbital–orbital distances to exhibit strong negative statistical correlations, which makes the hole bands robust to fluctuations of the orbital–orbital distances. As well as giving a concrete situation where the band structure averaging method can be meaningfully applied, this result shows that small band energy fluctuations can also be achieved with anisotropic orbitals, at least when they are aligned in this particular way. We expect for this research to inspire the search for other non-trivial conditions in which negligible band energy fluctuations can be achieved, and also provide directions for developing new materials with electronic properties resistant to thermal disorder.

## Acknowledgments

This research was supported by funding for the iCeMS-VISTEC Smart Materials Reserch Center located at VISTEC, Thailand. P P also acknowledges the support of grant no. TRG6280013 jointly funded by the Synchrotron Light Research Institute (SLRI) of Thailand and Thailand Research Fund (TRF).

## Appendix A. Tight-binding model

Our tight-binding model is constructed by noting that CuSCN consists of layers of Cu atoms, and that the unit cell contains two Cu atoms from adjacent layers (figure A1(A)). Referring to these layers as $L_1$ and $L_2$, respectively, we write the state of a single unit cell as a linear combination of Cu d orbitals, namely

$$|\mathbf{r}_j\rangle = \sum_{\mu=1}^{5} \left( c_\mu^{L_1} |\mu, \mathbf{r}_j, L_1\rangle + c_\mu^{L_2} |\mu, \mathbf{r}_j, L_2\rangle \right), \tag{A.1}$$

where $\mathbf{r}_j$ is the position vector for the unit cell, $|\mu, \mathbf{r}_j, L_1\rangle$ and $|\mu, \mathbf{r}_j, L_2\rangle$ represent d-orbitals with magnetic quantum number $\mu$ localized on the Cu atom from layers $L_1$ and $L_2$, respectively. The state of the system is given by the Bloch sum

$$|\mathbf{k}\rangle = \sum_{j=1}^{N} \mathrm{e}^{\mathrm{i}\mathbf{k}\cdot\mathbf{r}_j} |\mathbf{r}_j\rangle, \tag{A.2}$$

where $N$ is the number of unit cells in the crystal. Substituting (A.1) into the above shows that (A.2) can be written in the short-hand notation

$$|\mathbf{k}\rangle = \sum_{\alpha} a_\alpha |\alpha\rangle, \tag{A.3}$$

where the index $\alpha$ runs over all orbitals in the system, and $a_\alpha$ is an appropriate coefficient (for example, if $|\alpha\rangle = |\mu, \mathbf{r}_j, L_1\rangle$ for some $j$ and $\mu$, then $a_\alpha = {c_\mu}^{L_1} \exp(i\mathbf{k}\cdot\mathbf{r}_j)$). We write the tight-binding Hamiltonian as

$$H = H_0 + H_\mathrm{L} + H_\mathrm{I}, \tag{A.4}$$

where $H_0$ describes the system when localized at the d orbitals, $H_\mathrm{L}$ describes coupling between neighboring d-orbitals within the same layer and $H_\mathrm{I}$ describes coupling between d-orbitals of adjacent layers. $H_0$ can be immediately deduced as

$$H_0 = \sum_{j=1}^{N} \varepsilon_\mu \left( |\mu, \mathbf{r}_j, L_1\rangle \langle \mu, \mathbf{r}_j, L_1| + |\mu, \mathbf{r}_j, L_2\rangle \langle \mu, \mathbf{r}_j, L_2| \right), \tag{A.5}$$

where the expression is implicitly summed over $\mu = 1, 2, \ldots, 5$. The term $H_\mathrm{L}$ can be deduced by referring to figure A1(B),

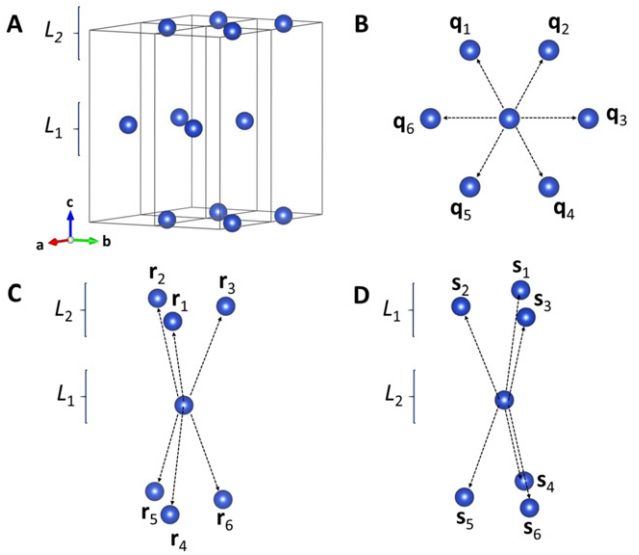


**Figure A1.** (A) Locations of the copper atoms (blue spheres) within the CuSCN unit cells. Unit cells are indicated by black lines. The layers $L_1$ and $L_2$ are indicated on the left. **a**, **b**, and **c** are the lattice vectors. By convention, the Cu atoms located on the bottom plane of the unit cell are assigned to the unit cell below. (B) Diagram showing nearest-neighbor positions for Cu atoms within the same plane. In the figure, the central Cu atom belong to the unit cell located at **0**, the origin of the crystal axes. The atoms labeled as $\mathbf{q}_1$, $\mathbf{q}_2$, $\mathbf{q}_3$, $\mathbf{q}_4$, $\mathbf{q}_5$, and $\mathbf{q}_6$ belong to the unit cells located at **b**, **b** + **a**, **a**, −**b**, −**b** − **a**, and −**a**, respectively. (C) and (D) show showing nearest-neighbor positions for Cu atoms laying in adjacent planes. In the figure, the central Cu atom belong to the unit cell located at the origin of the crystal axes. In (C), the central atom lies in the $L_1$ plane, and the atoms labeled as $\mathbf{r}_1$, $\mathbf{r}_2$, $\mathbf{r}_3$, $\mathbf{r}_4$, $\mathbf{r}_5$, and $\mathbf{r}_6$ belong to the unit cells located at −**b**, **0**, **a**, −**b** − **c**, −**c**, and **a** − **c**, respectively. In (D), the central atom lies in the $L_2$ plane, and the atoms labeled as $\mathbf{s}_1$, $\mathbf{s}_2$, $\mathbf{s}_3$, $\mathbf{s}_4$, $\mathbf{s}_5$, and $\mathbf{s}_6$ belong to the unit cells located at **b** + **c**, −**a** + **c**, **c**, **b**, −**a**, and **0**, respectively.

which shows the arrangement of nearest-neighbors for each Cu atom within the same layer. We obtain

$$H_{\mathrm{L}} = \sum_{j=1}^{N} t_{\mu'\mu}^{\mathbf{q}} \left( |\mu', \mathbf{r}_j + \mathbf{q}, L_1\rangle \langle \mu, \mathbf{r}_j, L_1| + |\mu', \mathbf{r}_j + \mathbf{q}, L_2\rangle \times \langle \mu, \mathbf{r}_j, L_2| \right) \tag{A.6}$$

where the expression is implicitly summed over $\mu = 1, 2, \ldots, 5$, $\mu' = 1, 2, \ldots, 5$, and $\mathbf{q} = \mathbf{b}, \mathbf{b} + \mathbf{a}, \mathbf{a}, -\mathbf{b}, -\mathbf{a} - \mathbf{b}, -\mathbf{a}$, where **a** and **b** are unit cell vectors parallel to the Cu layers. Here, $t_{\mu'\mu}{}^{\mathbf{q}}$ is a transfer integral for hole transfer from orbital $|\mu, \mathbf{r}_j, L_1\rangle$ to $|\mu', \mathbf{r}_j + \mathbf{q}, L_1\rangle$ (or equivalently, from $|\mu, \mathbf{r}_j, L_2\rangle$ to $|\mu', \mathbf{r}_j + \mathbf{q}, L_2\rangle$). Finally, the term $H_{\mathrm{I}}$ can be deduced by referring to figures A1(C) and (D), which show the nearest Cu atoms from the adjacent layers. We obtain

$$H_I = \sum_{j=1}^{N} \left( s_{\mu'\mu}^{\mathbf{v}} |\mu', \mathbf{r}_i + \mathbf{v}, L_2\rangle \langle \mu, \mathbf{r}_i, L_1| + s_{\mu'\mu}^{-\mathbf{v}} |\mu', \mathbf{r}_i - \mathbf{v}, L_1\rangle \times \langle \mu, \mathbf{r}_i, L_2| + s_{\mu'\mu}^{\mathbf{v}-\mathbf{c}} |\mu', \mathbf{r}_i + \mathbf{v} - \mathbf{c}, L_2\rangle \langle \mu, \mathbf{r}_i, L_1| + s_{\mu'\mu}^{-\mathbf{v}+\mathbf{c}} \times |\mu', \mathbf{r}_i - \mathbf{v} + \mathbf{c}, L_1\rangle \langle \mu, \mathbf{r}_i, L_2| \right) \tag{A.7}$$

where **c** is the unit cell vector perpendicular to the Cu layers, and the expression is implicitly summed over $\mu = 1, 2, \ldots, 5$, $\mu' = 1, 2, \ldots, 5$, and $\mathbf{v} = \mathbf{0}, \mathbf{a}, -\mathbf{b}$. The coefficients $s_{\mu'\mu}{}^{\mathbf{v}+\mathbf{c}}$ are the corresponding hole transfer integrals.

The band structure for the tight-binding Hamiltonian in (A.4) can be found by solving the secular equations

$$a_\beta \left( H_{\beta\beta} - E \right) + \sum_{\alpha} a_\alpha \left( H_{\alpha\beta} - E\delta_{\alpha\beta} \right) = 0, \tag{A.8}$$

where the indices $\alpha$ and $\beta$ run over all orbitals in the system, $a_\alpha$ and $a_\beta$ are the coefficients defined in equation (A.3), $\delta_{\alpha\beta}$ the Kronecker delta, and $E$ the **k**-dependent energy eigenvalue. Consider the case where $\beta = |\mu, \mathbf{r}_j, L_1\rangle$ for some $j$ and $\mu$. Then equation (A.8) becomes, after substituting in (A.6)–(A.7),

$$c_\mu^{L_1} \left( \varepsilon_\mu - E \right) + c_{\mu'}^{L_1} \mathrm{e}^{\mathrm{i}\mathbf{k}\cdot\mathbf{q}} t_{\mu'\mu}^{\mathbf{q}} + c_{\mu'}^{L_2} \left( \mathrm{e}^{\mathrm{i}\mathbf{k}\cdot\mathbf{v}} s_{\mu'\mu}^{\mathbf{v}} + \mathrm{e}^{\mathrm{i}\mathbf{k}\cdot(\mathbf{v}-\mathbf{c})} s_{\mu'\mu}^{\mathbf{v}-\mathbf{c}} \right) = 0, \tag{A.9}$$

where the second two terms are implicitly summed over $\mu' = 1, 2, \ldots, 5$, $\mathbf{q} = \mathbf{b}, \mathbf{b} + \mathbf{a}, \mathbf{a}, -\mathbf{b}, -\mathbf{a} - \mathbf{b}, -\mathbf{a}$, and $\mathbf{v} = \mathbf{0}, \mathbf{a}, -\mathbf{b}$. For the case where $\beta = |\mu, \mathbf{r}_j, L_2\rangle$, we obtain

$$c_\mu^{L_2} \left( \varepsilon_\mu - E \right) + c_{\mu'}^{L_2} \mathrm{e}^{\mathrm{i}\mathbf{k}\cdot\mathbf{q}} t_{\mu'\mu}^{\mathbf{q}} + c_{\mu'}^{L_1} \left( \mathrm{e}^{-\mathrm{i}\mathbf{k}\cdot\mathbf{v}} s_{\mu'\mu}^{\mathbf{v}} + \mathrm{e}^{-\mathrm{i}\mathbf{k}\cdot(\mathbf{v}-\mathbf{c})} s_{\mu'\mu}^{-(\mathbf{v}-\mathbf{c})} \right) = 0. \tag{A.10}$$

These equations can be written in matrix form as

$$\mathbf{S}\mathbf{c} = E\mathbf{c}, \tag{A.11}$$

where $\mathbf{c} = (c_1{}^{L_1}, c_2{}^{L_1}, c_3{}^{L_1}, c_4{}^{L_1}, c_5{}^{L_1}, c_1{}^{L_2}, c_2{}^{L_2}, c_3{}^{L_2}, c_4{}^{L_2}, c_5{}^{L_2})$, and the secular matrix has the form

$$\mathbf{S} = \begin{bmatrix} \mathbf{AA} & \mathbf{AB} \\ \mathbf{BA} & \mathbf{BB} \end{bmatrix} \tag{A.12}$$

Here, **AA** is the 5 × 5 matrix with elements

$$\mathbf{AA}_{\mu\mu'} = \begin{cases} \varepsilon_\mu + \mathrm{e}^{\mathrm{i}\mathbf{k}\cdot\mathbf{q}} t_{\mu\mu}^{\mathbf{q}} & \text{if } \mu' = \mu \\ \mathrm{e}^{\mathrm{i}\mathbf{k}\cdot\mathbf{q}} t_{\mu\mu'}^{\mathbf{q}} & \text{otherwise} \end{cases}, \tag{A.13}$$

**AB** is the 5 × 5 matrix with elements

$$\mathbf{AB}_{\mu'\mu} = \mathrm{e}^{\mathrm{i}\mathbf{k}\cdot\mathbf{v}} s_{\mu'\mu}^{\mathbf{v}} + \mathrm{e}^{\mathrm{i}\mathbf{k}\cdot(\mathbf{v}-\mathbf{c})} s_{\mu'\mu}^{\mathbf{v}-\mathbf{c}} \tag{A.14}$$

**BA** is the 5 × 5 matrix with elements

$$\mathbf{BA}_{\mu'\mu} = \mathrm{e}^{-\mathrm{i}\mathbf{k}\cdot\mathbf{v}} s_{\mu'\mu}^{\mathbf{v}} + \mathrm{e}^{-\mathrm{i}\mathbf{k}\cdot(\mathbf{v}-\mathbf{c})} s_{\mu'\mu}^{-(\mathbf{v}-\mathbf{c})} \tag{A.15}$$

and **BB** = **AA**. The matrix elements above are implicitly summed over $\mathbf{q} = \mathbf{b}, \mathbf{b} + \mathbf{a}, \mathbf{a}, -\mathbf{b}, -\mathbf{a} - \mathbf{b}, -\mathbf{a}$, and $\mathbf{v} = \mathbf{0}, \mathbf{a}, -\mathbf{b}$ as appropriate. The eigenvalue problem in equation (A.11) yields 10 bands, each arising from one of the 10 d-orbitals contained within each unit cell of CuSCN.

The transfer integrals $t_{\mu'\mu}{}^{\mathbf{q}}$ and $s_{\mu'\mu}{}^{\mathbf{v}}$ are treated as Slater–Koster integrals [26]. For completeness, the explicit forms of the transfer integrals used in this paper are shown in supporting information VI. Our tight-binding model contains 11 free parameters: five d-orbital energies ($\varepsilon_1$, $\varepsilon_2$, $\varepsilon_3$, $\varepsilon_4$, $\varepsilon_5$), three within-layer interaction terms [$(dd\sigma)_0$, $(dd\pi)_0$, $(dd\delta)_0$], and three between-layer interaction terms [$(dd\sigma)_1$,

$(dd\pi)_1$, $(dd\delta)_1$]. These parameters were fitted using an in-house code written in a combination of R and C++ languages. Eigenvalues of the tight-binding Hamiltonian were computed using the Eigen library for C++ [29]. Hermiticity of the tight-binding Hamiltonians was confirmed by checking whether the imaginary parts of the eigenvalues were 0 at each $k$-point. The fitted values of the parameters are shown in supporting information V.

## Appendix B. Stochastic network model

In this section, we first obtain a general expression for OD, the mean-square displacement of $E'$ from zero band energy displacement in the stochastic network model. Following this, we reduce the general expression to the specific one shown in equation (7) of the main paper.

### *B.1. General expression for the mean square energy displacement*

Let $\mathbf{r}_1, \mathbf{r}_2, \ldots, \mathbf{r}_N$ be the positions of the nodes in the absence of disorder, and let $\mathbf{u}_1, \mathbf{u}_2, \ldots, \mathbf{u}_N$ be the positions in the presence of disorder. Explicitly, we have

$$\mathbf{u}_i = \mathbf{r}_i + \mathbf{X}_i \tag{B.1}$$

where $\mathbf{X}_i$ is a random vector. The components of $\mathbf{X}_i$ follow a Gaussian distribution with mean 0 and variance $\sigma^2$. The components are assumed to be statistically independent of each other, with no dependence between random vectors belonging to different atoms. Because these random vectors are assumed to be 'small' (in the sense that $\sigma$ is small), the Hamiltonian in the presence of disorder can be written as

$$H(\mathbf{u}_1, \mathbf{u}_2, \ldots, \mathbf{u}_N) = H(\mathbf{r}_1, \mathbf{r}_2, \ldots, \mathbf{r}_N) + H', \tag{B.2}$$

where $H'$ is a perturbation. Providing that the stochastic network model is set-up in such a way that degenerate states do not appear (see appendix C), the first-order correction to the energy $E'$ is $E' = \langle\psi|H'|\psi\rangle$, where $|\psi\rangle$ is the state of the system in the absence of disorder. Inserting equation (3) of the main text gives

$$E' = \sum_{\alpha,\beta=1}^{N} c_\alpha c_\beta H'_{\alpha\beta}, \tag{B.3}$$

Note that the wave function coefficients $c_\alpha$ are real by assumption. The mean-square displacement of $E'$ from 0 is defined as

$$\mathrm{OD} = \left\langle E'^2 \right\rangle, \tag{B.4}$$

where the angular brackets, which should not be confused with the angular brackets used to denote quantum states, indicate averaging over all realizations of the structural disorder. Inserting (B.3) into (B.4), gives

$$\mathrm{OD} = \sum_{\alpha,\beta=1}^{N} c_\alpha^2 c_\beta^2 \left\langle H'^2_{\alpha\beta} \right\rangle + \sum_{\alpha,\beta=1}^{N} \sum_{\delta,\gamma=1}^{N} c_\alpha c_\beta c_\delta c_\gamma \left\langle H'_{\alpha\beta} H'_{\delta\gamma} \right\rangle \tag{B.5}$$

as our general expression for OD. In the language of statistics, the quantities $\langle {H'^2}_{\alpha\beta} \rangle$ and $\langle {H'}_{\alpha\beta} {H'}_{\delta\gamma} \rangle$ are referred to as variances and covariances, respectively. Covariances are proportional to correlations.

### *B.2. Perturbation matrix elements*

In order to obtain equation (7) from the general expression (B.5), we need expressions for the perturbation Hamiltonian matrix elements ${H'}_{\alpha\beta}$. To obtain these expressions, note that in the presence of structural disorder, the full Hamiltonian can be written in one of two ways. One way is

$$H(\mathbf{u}_1, \mathbf{u}_2, \ldots, \mathbf{u}_N) = H(\mathbf{r}_1, \mathbf{r}_2, \ldots, \mathbf{r}_N) + H', \tag{B.6}$$

as in equation (B.2), where (see equation (3) of the main text),

$$H(\mathbf{r}_1, \mathbf{r}_2, \ldots, \mathbf{r}_N) = \varepsilon \sum_{\alpha=1}^{N} |\alpha\rangle \langle\alpha| + \sum_{\alpha\sim\beta} g\left(r_{\alpha\beta}\right) |\alpha\rangle \langle\beta|, \tag{B.7}$$

and the notation $\alpha \sim \beta$ means that the summation is over all pairs of nodes which are connected. The other way to write the full Hamiltonian is (see equation (4) of the main text)

$$H(\mathbf{u}_1, \mathbf{u}_2, \ldots, \mathbf{u}_N) = \varepsilon \sum_{\alpha=1}^{N} |\alpha\rangle \langle\alpha| + \sum_{\alpha\sim\beta} g\left(r_{\alpha\beta} + \Delta r_{\alpha\beta}\right) |\alpha\rangle \langle\beta| \tag{B.8}$$

Comparing equations (B.7) and (B.8) shows that

$$H' = \sum_{\alpha\sim\beta} \left( g\left(r_{\alpha\beta} + \Delta r_{\alpha\beta}\right) - g\left(r_{\alpha\beta}\right) \right) |\alpha\rangle \langle\beta|. \tag{B.9}$$

An expression for the term in brackets can be found by performing a Taylor's series expansion. Expanding $g$ to first-order in the $\Delta$-terms gives

$$g\left(r_{\alpha\beta} + \Delta r_{\alpha\beta}\right) - g\left(r_{\alpha\beta}\right) = R_{\alpha\beta} \Delta r_{\alpha\beta}, \tag{B.10}$$

where $R_{\alpha\beta} = (\mathrm{d}g/\mathrm{d}\Delta r_{\alpha\beta})_{\Delta r_{\alpha\beta}=0}$. The perturbation Hamiltonian elements are therefore equal to

$$H'_{\alpha\beta} = \begin{cases} R_{\alpha\beta}\Delta r_{\alpha\beta} & \text{if } \alpha \sim \beta, \\ 0 & \text{otherwise.} \end{cases} \tag{B.11}$$

### *B.3. Averaging over the perturbation elements*

We now turn to the averages $\langle {H'^2}_{\alpha\beta} \rangle$ and $\langle {H'}_{\alpha\beta} {H'}_{\delta\gamma} \rangle$, which are contained the general expression in (B.5). From (B.11) we obtain

$$\left\langle H'^2_{\alpha\beta} \right\rangle = R^2_{\alpha\beta} \left\langle \Delta r^2_{\alpha\beta} \right\rangle \tag{B.12}$$

and

$$\left\langle H'_{\alpha\beta} H'_{\delta\gamma} \right\rangle = R_{\alpha\beta} R_{\delta\gamma} \left\langle \Delta r_{\alpha\beta} \Delta r_{\delta\gamma} \right\rangle. \tag{B.13}$$

respectively. The quantities $\langle {\Delta r_{\alpha\beta}}^2 \rangle$ and $\langle \Delta r_{\alpha\beta} \Delta r_{\gamma\delta} \rangle$ in equations (B.12) and (B.13) are computed as follows. By definition, we have $r_{\alpha\beta} + \Delta r_{\alpha\beta} = |(\mathbf{r}_\alpha + \mathbf{X}_\alpha) - (\mathbf{r}_\alpha + \mathbf{X}_\beta)|$.

Expanding the right-hand side of this expression to first-order in the components of $\mathbf{X}_\alpha$ and $\mathbf{X}_\beta$ gives, after some algebra,

$$\Delta r_{\alpha\beta} = \frac{1}{r_{\alpha\beta}} \left(\mathbf{r}_\alpha - \mathbf{r}_\beta\right) \cdot \left(\mathbf{X}_\alpha - \mathbf{X}_\beta\right) \tag{B.14}$$

Recalling that the mean and variance of each component of $\mathbf{X}_\alpha$ and $\mathbf{X}_\beta$ is 0 and $\sigma^2$, respectively, we immediately obtain

$$\langle \Delta r_{\alpha\beta} \rangle = 0, \tag{B.15}$$

$$\left\langle \Delta r_{\alpha\beta}^2 \right\rangle = 2\sigma^2. \tag{B.16}$$

For the case of three nodes $\alpha$, $\beta$, and $\gamma$ connected sequentially (i.e., $\alpha$ is connected to $\beta$, and $\beta$ is connected to $\gamma$), we obtain

$$\langle \Delta r_{\alpha\beta} \Delta r_{\beta\gamma} \rangle = -\frac{\sigma^2}{r_{\alpha\beta} r_{\beta\gamma}} \left(\mathbf{r}_\alpha - \mathbf{r}_\beta\right) \cdot \left(\mathbf{r}_\beta - \mathbf{r}_\gamma\right) = \sigma^2 \cos \chi_{\alpha\beta\gamma}, \tag{B.17}$$

where $\chi_{\alpha\beta\gamma}$ is the angle $\alpha\beta\gamma$. For the case of two pairs of distinct nodes ($\alpha$, $\beta$) and ($\gamma$, $\delta$) we have

$$\langle \Delta r_{\alpha\beta} \Delta r_{\gamma\delta} \rangle = 0. \tag{B.18}$$

Substituting these expressions into (B.12) and (B.13), we obtain

$$\left\langle H'^2_{\alpha\beta} \right\rangle = 2R^2_{\alpha\beta}\sigma^2 \tag{B.19}$$

and

$$\left\langle H'_{\alpha\beta} H'_{\delta\gamma} \right\rangle = \begin{cases} \sigma^2 R_{\alpha\beta} R_{\beta\gamma} \cos \chi_{\alpha\beta\gamma} & \text{if } \delta = \beta \\ 0 & \text{otherwise} \end{cases} \tag{B.20}$$

respectively. Substituting (B.19) and (B.20) into (B.5) yields

$$\mathrm{OD} = 2\sigma^2 \sum_{\alpha\sim\beta} c_\alpha^2 c_\beta^2 R_{\alpha\beta} + \sigma^2 \sum_{\alpha\sim\beta\sim\gamma} c_\alpha c_\beta^2 c_\gamma R_{\alpha\beta} R_{\beta\gamma} \cos \chi_{\alpha\beta\gamma}, \tag{B.21}$$

which is equivalent to equation (7) of the main paper. Note that in (B.21) (or equation (7)), each pair of connected nodes appears twice in the first sum. Similarly, each triple of nodes connected in series appears twice in the second sum.

## Appendix C. Computation of the OD term

We computed equation (B.21) for three types of networks. The first type consists of a straight row of 108 nodes connected in sequence. The second type consists of a single plane of 108 nodes connected in the four-fold pattern shown by the purple connections figure 4(A). The third type consists of the same plane of 108 nodes, but connected in the six-fold pattern shown by the green and purple connections in figure 4(A). The first two types were used to perform the calculations 'A strong, B off' and 'A off, B strong', respectively, from figure 4(B). The third type was used to perform the calculations 'A strong, B strong' and 'A strong, B weak'. In each case, the Hamiltonian in equation (4) was calculated with the node energies $\varepsilon$ set to 0 (which has no effect on the calculation), and the coefficients of the ground state wave function were obtained by computing the eigenvectors of the Hamiltonian. For each of the four networks considered here, the ground state was not degenerate and all ground state wave function coefficients had the same sign, justifying the use of ordinary perturbation theory as well as the assumptions made on the wave function in equation (4).

## ORCID iDs

Daniel M Packwood https://orcid.org/0000-0001-9387-728X
Pichaya Pattanasattayavong https://orcid.org/0000-0001-6374-1840

## References

[1] Maurer R K, Freysoldt C, Reilly A M, Brandenburg J G, Hofmann O T, Bjorkman T, Lebegue S and Tkatchenko A 2019 Advances in Density-Functional Calculations for Materials Modeling *Annu. Rev. Mater. Res.* **49** 3.1–30
[2] Pribram-Jones A, Gross D A and Burke K 2015 DFT: A Theory Full of Holes? *Annu. Rev. Phys. Chem.* **66** 283–304
[3] Gibbs Z M, Kim H, Wang H, White R L, Drymiotis F, Kaviany M and Snyder G J 2013 Temperature dependent band gap in PbX (X = S, Se, Te) *Appl. Phys. Lett.* **103** 262109–14
[4] Stern R and Madsen G K H 2016 *Ab initio* investigation of the anomalous phonon softening in FeSi *Phys. Rev.* B **94** 144304–11
[5] Delaire O, Marty K, Stone M B, Kent P R C, Lucas M S, Abernathy D L, Mandrus D and Sales B C 2011 Phonon softening and metallization of a narrow-gap semiconductor by thermal disorder *Proc. Natl Acad. Sci. USA* **108** 4725–30
[6] Nomura K, Ohta H, Takagi A, Kamiya T, Hirano M and Hosono H 2004 Room-temperature fabrication of transparent flexible thin-film transistors using amorphous oxide semiconductors *Nature* **432** 488–92
[7] Yu X, Marks T J and Facchetti A 2015 Metal oxides for optoelectronic applications *Nat. Mater.* **15** 383–96
[8] Zhang K H L, Xi K, Blamire M G and Egdel R G 2016 P-type transparent conducting oxides *J. Phys.: Condens. Matter* **28** 383002–12
[9] Noriega R, Rivnay J, Vandewal K, Koch F P V, Stingelin N, Smith P, Toney M F and Salleo A 2013 A general relationship between disorder, aggregation and charge transport in conjugated polymers *Nat. Mater.* **12** 1038–44
[10] Narushima S, Orita M, Hirano M and Hosono H 2002 Electronic structure and transport properties in the transparent amorphous oxide semiconductor $2CdO{\cdot}GeO_2$ *Phys. Rev.* B **66** 035203–11
[11] Nomura K, Kamiya T, Ohta H, Uruga T, Hirano M and Hosono H 2007 Local coordination structure and electronic structure of the large electron mobility amorphous oxide semiconductor In-Ga-Zn-O: Experiment and *ab initio* calculations *Phys. Rev.* B **75** 035212–7
[12] Pattanasattayavong P, Promarak V and Anthopoulos T D 2017 Electronic Properties of Copper(I) Thiocyanate (CuSCN) *Adv. Electron. Mater.* **3** 1600378–90
[13] Wijeyasinghe N, Regoutz A, Eisner F, Du T, Tsetseris L, Lin Y-H, Faber H, Pattanasattayavong P, Li J, Yan F, McLachlan M A, Payne D J, Heeney M and Anthopoulos T D 2017 Copper(I) Thiocyanate (CuSCN) Hole-Transport Layers Processed from Aqueous Precursor Solutions and Their Application in Thin-Film Transistors and High Efficient Organic and Organometal Halide Perovskite Solar Cells *Adv. Funct. Mater.* **27** 1701818–30

[14] Pattanasattayavong P, Yaacobi-Gross N, Zhao K, Oliver G, Ndjawa N, Li J, Yan F, O'Regan B C, Amassian A and Anthopoulos T D 2013 Hole-Transporting Transistors and Circuits Based on the Transparent Inorganic Semiconductor Copper(I) Thiocyanate (CuSCN) Processed from Solution at Room Temperature *Adv. Mater.* **25** 1504–9

[15] Perumal A, Faber H, Yaacobi-Gross N, Pattanasattayavong P, Burgess C, Jha S, McLachlan M A, Stavrinou P N, Anthopoulos T D and Bradley D D C 2015 High-efficiency, solution-processed, multilayer phosphorescent organic light-emitting diodies with a copper thiocyanate hole-injection/hole-transport Layer *Adv. Mater.* **27** 93–100

[16] Smith D L and Saunders V I 1982 Preparation and structure refinement of the 2H polytype of beta-copper(I) thiocyanate *Acta Cryst.* B **38** 907–9

[17] Kresse G and Furthmuller J 1996 Efficient iterative schemes for *ab initio* total energy calculations using a plane-wave basis set *Phys. Rev.* B **54** 11169–86

[18] Perdew J P, Burke K and Ernzerhof M 1996 Generalized Gradient Approximation Made Simple *Phys. Rev. Lett.* **77** 3865–8

[19] R Core Team 2019 *R: A Language and Environment for Statistical Computing* (Vienna: R Foundation for Statistical Computing)

[20] David C C and Jacobs D J 2014 Principal component analysis: a method for determining the essential dynamics of proteins *Protein Dynamics* ed Livesay D R (Humana Press) pp 193–226

[21] Jaffe J E, Kaspar T C, Droubay T C, Varga T, Bowden M E and Exarhos G J 2014 Electronic and Defect Structures of CuSCN *J. Phys. Chem.* C **114** 9111–7

[22] Chen K J, Laurent A D, Boucher F, Odobel F and Jacquemin D 2016 Determining the most promising anchors for CuSCN: *ab initio* insights towards p-type DSSCs *J. Mater. Chem.* A **4** 2217–27

[23] Perdew J P, Yang W, Burke K, Yang Z, Gross E K U, Scheffler M, Scuseria G E, Henderson T M, Zhang I Y, Ruzsinszky A, Peng H, Sun J, Trushin E and Gorling A 2017 Understanding band gaps of solids in generalized Kohn-Sham theory *Proc. Natl Acad. Sci. USA* **114** 2801–6

[24] Tsetseris L 2016 Copper thiocyanate: polytypes, defects, impurities, and surfaces *J. Phys.: Condens. Matter* **28** 295801–8

[25] Varshni Y P 1967 Temperature dependence of the energy gap in semiconductors *Physica* **34** 149–54

[26] Slater J C and Koster G F 1954 Simplified LCAO Method for the Periodic Potential Problem *Phys. Rev.* **94** 1498–524

[27] Ridolfi E, Le D, Rahman T S, Mucciolo E R and Lewenkopf C H 2015 A tight-binding model for $MoS_2$ monolayers *J. Phys.: Condens. Matter* **27** 365501

[28] Packwood D M, Reaves K T, Federici F L, Katzgraber H G and Teizer W 2013 Two-dimensional molecular magnets with weak topological invariant magnetic moments: mathematical prediction of targets for chemical synthesis *Proc. R. Soc.* A **469** 20130373–86

[29] Eigen Development Team 2010 *Eigen v3* http://eigen.tuxfamily.org